Deep–Sea Research I 156 (2020) 103141

Contents lists available at ScienceDirect

Deep-Sea Research Part I

journal homepage: http://www.elsevier.com/locate/dsri

# Size-fractionated biomass and primary productivity of Sargasso Sea phytoplankton

Bridget E. Cotti-Rausch [a], Michael W. Lomas [b], Eric M. Lachenmyer [a], Emily G. Baumann [a], Tammi L. Richardson [a,c,*]

[a] School of the Earth, Ocean and Environment, University of South Carolina, 712 Main St., Columbia, SC, 29208, USA
[b] Bigelow Laboratory for Ocean Sciences, 60 Bigelow Dr., East Boothbay, ME, 04544, USA
[c] Department of Biological Sciences, University of South Carolina, 715 Sumter St., Columbia, SC, 29208, USA

ARTICLE INFO

*Keywords:*
Size
C:Chl
Flow cytometry
Carbon
$P^{chl}$

ABSTRACT

The size structure of phytoplankton communities greatly influences the function of pelagic food webs and, ultimately, the flux of material from the surface ocean to the deep sea. While the biomass and taxonomic composition of organisms in a specific size class are important characteristics of a food web, the activity of that size fraction is more directly relevant to trophic dynamics and biogeochemical cycling. Even if a size class dominates cell abundance or biomass, does it necessarily contribute the most to total primary productivity (PP)? We asked this question for phytoplankton communities from the Sargasso Sea. The picophytoplankton (0.7–2 μm) accounted for 53–85% of the total integrated chl-*a* and 46–99% or more of the total integrated PP. The microphytoplankton (20–200 μm) were responsible for up to 38% of the total PP, but accounted for no more than 22% of total chl-*a*. Variations in the picophytoplankton size-class explained 84% of the variance in total integrated chl-*a* and 87% of the variance in total PP. Size-dependent relative contributions to chl-*a* versus PP varied with depth, with differences generally driven by vertical variations in C:chl-*a* ratios and chl-specific rates of PP. Use of the relative contributions of picophytoplankton to biomass as a predictor of their contributions to total primary productivity resulted in an average underestimate of ~7%.

## 1. Introduction

The size structure of phytoplankton communities greatly influences the function of pelagic food webs and, ultimately, the flux of particulate material from the surface ocean to the deep sea (Ryther, 1969; Malone, 1980; Legendre and Le Fèvre, 1989, 1991; Tremblay and Legendre, 1994; Rivkin et al., 1996; Marañon et al., 2001). Ecosystems dominated by large phytoplankton, such as coastal or upwelling regions, have short, efficient food webs that export a high percentage of primary productivity (PP) to higher trophic levels or deeper waters (Michaels and Silver, 1988; McManus, 1991; Boyd and Newton, 1995). In oligotrophic subtropical gyres, small phytoplankton dominate, microbial remineralization rates are high (Azam, 1998; Robinson and Williams, 2005), and multiple trophic transfers from small to larger grazers often result in the export of just 1–2% of the PP (Pomeroy, 1974; Azam et al., 1983, 1993; Ducklow et al., 1986; Pomeroy et al., 2007). Shorter, more direct routes for small phytoplankton export, e.g., by gelatinous zooplankton feeding directly on small cells and/or large zooplankton feeding on aggregates of picoplankton, have been described recently (Ebersbach and Trull, 2008; Ebersbach et al., 2014; Sutherland et al., 2010; Wilson and Steinberg, 2010; Motwani and Gorokhova, 2013; Richardson, 2019), further illustrating the diverse pathways by which small phytoplankton undergo trophic transformation.

While the structure of a food web is important, it is not only the biomass contained within a size fraction but also the activities (specific rates) associated with that fraction that are directly relevant to trophic dynamics and biogeochemical cycling. Much of our understanding of size-dependent processes is from concurrent measurements of size-fractionated chlorophyll-*a* (chl-*a*) biomass and size-fractionated PP. Early work focused on the inherent differences between small and large phytoplankton based on surface area to volume ratio and how differences in this ratio may result in size-dependent rates of photosynthesis, nutrient uptake, and growth (Malone, 1971; Bruno et al., 1983; Furnas, 1983; Glover et al., 1985). Later work addressed relationships between phytoplankton size, PP, and carbon export (Legendre et al., 1993; Jochem and Zeitzschel, 1993; Tremblay and Legendre, 1994). Studies of

* Corresponding author. School of the Earth, Ocean and Environment, University of South Carolina, 712 Main St., Columbia, SC, 29208, USA.
*E-mail address:* richardson@biol.sc.edu (T.L. Richardson).

https://doi.org/10.1016/j.dsr.2019.103141
Received 15 August 2019; Accepted 18 October 2019
Available online 25 October 2019

**Table 1**
Dates and locations of sampling in the Sargasso Sea in the spring and summer of 2011 and 2012. Three stations were sampled on cruises AE1102, AE1118, and AE1219: the center and edge of a mesoscale eddy and the Bermuda Atlantic Time-series Study (BATS) station. Two stations were sampled on AE1206 (the center of a cyclonic eddy and the BATS station).

| Cruise Number | Eddy Type (eddy name) | Season | Dates | Stations Sampled | Coordinates (Latitude, Longitude) | Number of *in situ* experiments |
|---|---|---|---|---|---|---|
| AE1102 | Anticyclone (AC1) | Spring | 24 Feb – 5 March 2011 | Center | 29° 42′ N, 64° 06′ W | 1 |
| | | | | Edge | 30° 30′ N, 64° 08′ W | 1 |
| | | | | BATS | 31° 40′ N, 64° 10′ W | 1 |
| AE1118 | Cyclone (C1) | Summer | 22 July – 5 August 2011 | Center | 30° 49′ N, 65° 47′ W | 2 |
| | | | | Edge | 31° 17′ N, 64° 55′ W | 1 |
| | | | | BATS | 31° 40′ N, 64° 10′ W | 2 |
| AE1206 | Cyclone (C2) | Spring | 15–23 Mar 2012 | Center | 32° 50′ N, 63° 29′ W | 2 |
| | | | | BATS | 31° 40′ N, 64° 10′ W | 2 |
| AE1219 | Anticyclone (AC2) | Summer | 19–31 July 2012 | Center | 33° 30′ N, 64° 27′ W | 2 |
| | | | | Edge | 32° 23′ N, 64° 22′ W | 2 |
| | | | | BATS | 31° 40′ N, 64° 10′ W | 2 |

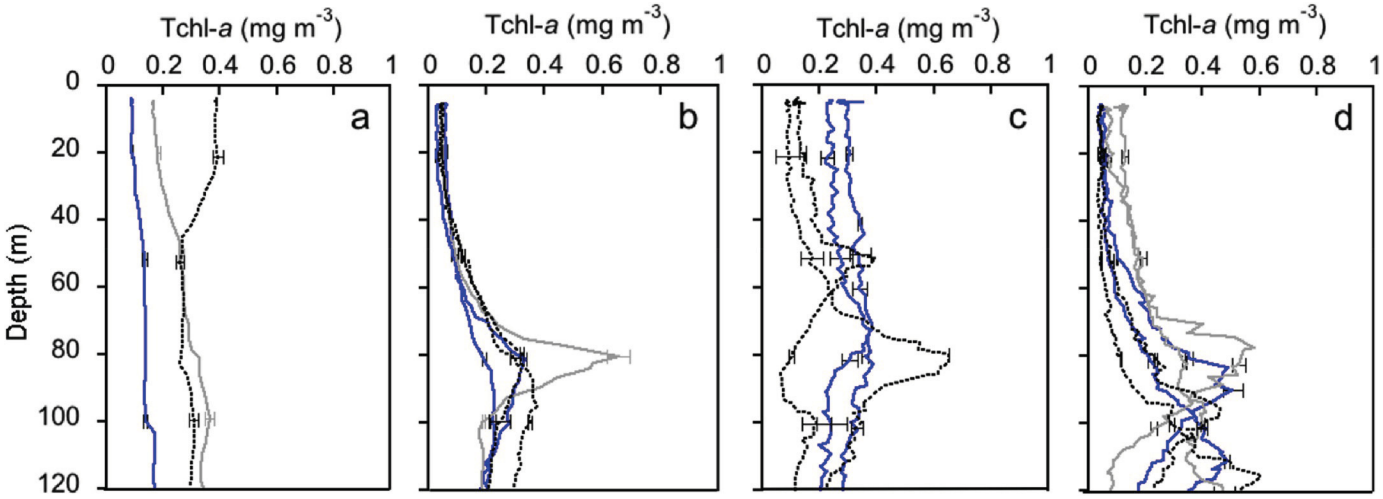


**Fig. 1.** Total chlorophyll-*a* (Tchl-*a*) profiles calculated from CTD fluorescence profiles calibrated against direct measurements of chl-*a* at 3 to 4 depths. Error bars represent standard deviations (n = 3) of direct measurements at discrete depths. Casts were done before dawn at stations at the center (blue) or edge (grey) of each eddy and at the Bermuda Atlantic Time-series Study site (dashes) in a) spring 2011, b) summer 2011, c) spring 2012 and d) summer 2012. In spring 2012, the edge of eddy C2 was not sampled. Profiles with the same symbol on the same panel represent duplicate casts performed at the same station within 48 h of each other (where applicable).

proportional contributions of varying phytoplankton size fractions to biomass and PP were relatively rare, until the pioneering work of Marañón and colleagues (e.g., Marañón et al., 2001, 2003; Fernandez et al., 2003) who examined size-based contributions to biomass and PP over a variety of ecological domains, including the eastern North Atlantic and South Atlantic oligotrophic gyres. In the oligotrophic regions, they found significant variability in PP that was not accompanied by changes in the size structure of the phytoplankton community (Marañón et al., 2001). Variations in PP were instead the result of dynamics within the microbial community and shifts in the relative contributions of *Synechococcus* and picoeukaryotes vs. *Prochlorococcus* to total phytoplankton biomass (Marañón et al., 2003).

Here, our objective was to determine whether size-specific relative contributions to biomass (as chl-*a*) were proportional to contributions to total PP for phytoplankton from the Sargasso Sea. We used data collected on four cruises in 2011 and 2012 as part of a larger program ("Trophic BATS") that examined the role of plankton size and taxonomic composition in carbon cycling through food webs of this region (see Cotti-Rausch et al., 2016; De Martini, 2016). We also explored the implications of using size-fractionated biomass as a way to estimate size-fractionated rates of PP for food web models as has been done when data on size-fractionated rates of PP were not available (e.g., Richardson et al., 2006).

## 2. Materials and methods

### 2.1. Study sites and sampling

We collected data on four cruises in the Sargasso Sea on the R/V *Atlantic Explorer* in the spring and summer of 2011 and 2012 (Table 1). The circulation of the Sargasso Sea is strongly influenced by mesoscale eddies (Olson, 1991), thus we targeted our sampling to take these eddies into account. On three of the cruises (AE1102, AE1108, and AE1219), we sampled and performed *in situ* experiments at three stations: the

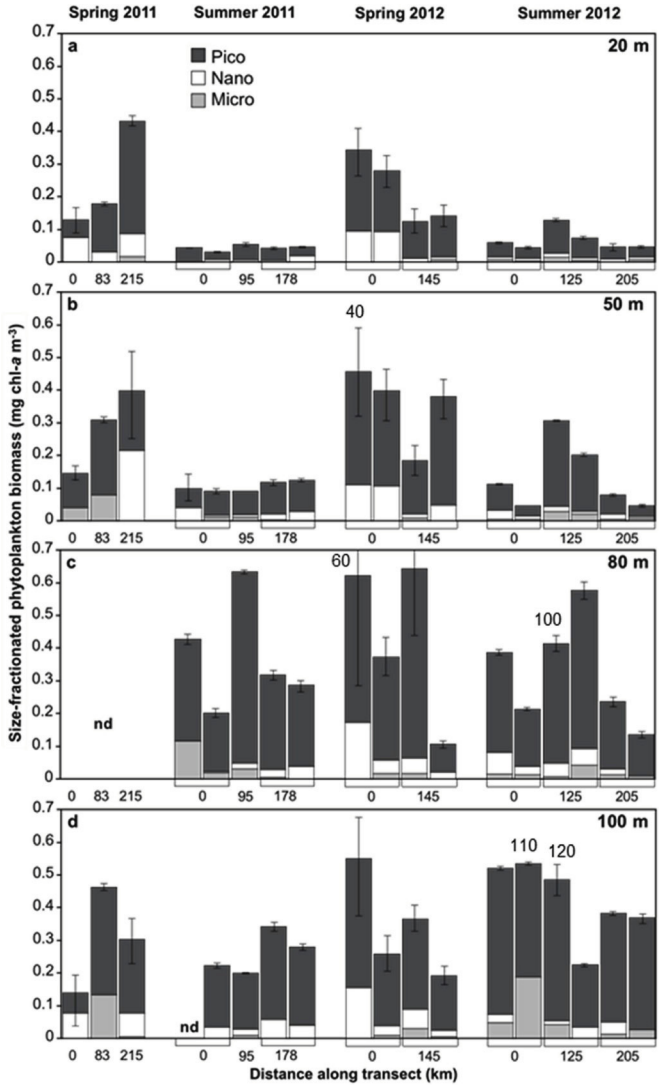


**Fig. 2.** Size-fractionated phytoplankton biomass (chl-*a*; mg $m^{-3}$) for the picophytoplankton (Pico, 0.7–2 μm), nanophytoplankton (Nano, 2–20 μm) and microphytoplankton (Micro, 20–200 μm) at: a) 20 m, b) 50 m, c) 80 m, and d) 100 m, unless otherwise noted by values over individual bars. Cruise transects began at an eddy's center (0 km) and progressed to an edge station (except for Spring 2012) then to the Bermuda Atlantic Time-series Study site (farthest point along each transect). Error bars represent the standard deviation of triplicate measurements of total chl-*a* at each depth. Standard deviations for individual size fractions ranged from 6% to 30% of the average depending on fraction, depth, and station.

**Table 2**
Average (±standard deviation, where possible) size-fractionated and total integrated (to 100 m) chlorophyll-*a* (chl-*a*) biomass for all cruises and stations. Phytoplankton size-fractions are abbreviated as follows: Pico = picophytoplankton, 0.7–2 μm; Nano = nanophytoplankton, 2–20 μm; Micro = microphytoplankton, 20–200 μm and Total = 0.7–200 μm. Values in parentheses are % contributions of each size class to total chl-*a* biomass.

| Cruise (Eddy) | Date | Station | Pico Biomass (mg chl-*a* $m^{-2}$) | Nano Biomass (mg chl-*a* $m^{-2}$) | Micro Biomass (mg chl- *a* $m^{-2}$) | Total Biomass (mg chl-*a* $m^{-2}$) |
|---|---|---|---|---|---|---|
| AE1102 (AC1) | Spring 2011 | Center | 8 (53%) | 5 (35%) | 2 (12%) | 15 |
| | | Edge | 23 (72%) | 2 (6%) | 7 (22%) | 32 |
| | | BATS | 25 (65%) | 12 (32%) | 1 (3%) | 38 |
| AE1118 (C1) | Summer 2011 | Center | 10 ± 1 (75%) | 1 ± 1 (9%) | 2 ± 2 (16%) | 13 ± 3 |
| | | Edge | 20 (85%) | 1 (7%) | 2 (8%) | 23 |
| | | BATS | 13 ± 1 (81%) | 3 ± 1 (16%) | 1 ± 0 (3%) | 17 ± 1 |
| AE1206 (C2) | Spring 2012 | Center | 28 ± 4 (74%) | 10 ± 3 (25%) | 0 ± 1 (1%) | 38 ± 6 |
| | | BATS | 22 ± 6 (84%) | 3 ± 0 (11%) | 1 ± 0 (5%) | 26 ± 6 |
| AE1219 (AC2) | Summer 2012 | Center | 13 ± 4 (76%) | 2 ± 1 (11%) | 2 ± 2 (13%) | 17 ± 5 |
| | | Edge | 24 ± 4 (83%) | 3 ± 1 (9%) | 2 ± 1 (8%) | 29 ± 5 |
| | | BATS | 10 ± 2 (81%) | 1 ± 1 (9%) | 1 ± 0 (10%) | 12 ± 3 |

center and edge of a mesoscale eddy (AC1, C1, and AC2; see Table 1) and at the Bermuda Atlantic Time-series Study (BATS) site. On cruise AE1206 we sampled only at the center of a cyclonic eddy (C2) and at BATS. Eddies were identified using satellite-derived sea level anomaly (SLA) data as described in Cotti-Rausch et al. (2016). One eddy per cruise was identified, and the position of the ship within the eddy was confirmed daily with SLA data. The influence of these mesoscale features is not addressed here but is the topic of a separate publication (Cotti-Rausch et al., 2016). At each station, vertical profiles of fluorescence (Chelsea-MkIII Aquatracka), temperature (SBE 3-02/F) and salinity (SBE 4-02/0) were performed using a Sea Bird CTD (Sea-Bird Electronics, SBE-09 *plus*).

### 2.1.1. Pre-dawn CTD casts

Before dawn on each sampling day we conducted a CTD cast to 200 m with a 24-bottle Niskin rosette (General Oceanics Model 1016-24) to characterize the physical structure of the water column and to collect water for measurements of size-fractionated chl-*a* biomass and rates of size-fractionated PP. The number of casts, and therefore number of experiments, varied by cruise depending on the time available for *in situ* deployments (see Table 1). On each cast, we collected water at 3 to 4 depths (20 m, 50 m, the deep fluorescence maximum (usually ~80 m), and 100 m). Replicate Niskin bottle samples (n = 2 - 3) were taken at each depth. For sample collection, opaque 10-l polycarbonate bottles were pre-rinsed with sample water and filled on deck through opaque tubing to avoid light shock. Water samples were pre-screened through a 200-μm Nitex mesh to remove large grazers. Further handling of the samples was done in dim light or under red light. We converted fluorescence profiles to chl-*a* profiles using fluorescence/chl-*a* ratios calculated from discrete measurements of chl-*a* at each sampling depth. Intermediate values were determined by linear interpolation between discrete sampling points.

We determined phytoplankton biomass by filtering triplicate aliquots (1–2 l) of pre-screened water through GF/F filters. This provided total chl-*a* in the size fraction 0.7–200 μm. The biomass of three size classes of phytoplankton, the picophytoplankton (0.7–2 μm), the nanophytoplankton (2–20 μm) and the microphytoplankton (20–200 μm), was quantified by differential filtration as follows. First, triplicate aliquots (1–2 l) of pre-screened water were filtered onto 2 μm Nuclepore filters (= 2–200 μm) and picophytoplankton biomass was calculated by subtracting the 2–200 μm biomass from the total chl-*a* value. Triplicate aliquots of pre-screened water were also filtered through a 20 μm Nitex mesh, then onto a GF/F filter to yield the 0.7–20 μm fraction. Biomass of the nanophytoplankton size class was calculated by subtracting the picophytoplankton biomass from the 0.7–20 μm biomass. Microphytoplankton biomass was determined by subtracting the 0.7–20 μm biomass from the total chl-*a* value. All filters were folded, placed in 1.5 ml cryotubes, and frozen at −80 °C for later analysis at the University of South Carolina as described in the Analytical Methods section.

### 2.1.2. Mid-day CTD casts

At local noon at each station we did CTD casts to 1000 m. We took water samples (1–2 l) from 6 to 7 depths (usually 1, 20, 50, 80, 100, 150, 200 m) for measurement of total chl-*a* biomass (as in 2.1.1) by HPLC (see section 2.3). Separate samples were preserved in paraformaldehyde (0.5% final concentration) for analysis of the abundance and carbon biomass of the picocyanobacteria (*Prochlorococcus* and *Synechococcus*), picoeukaryotes and nanoeukaryotes by flow cytometry. Carbon biomass values were used to estimate C:chl-*a* ratios (g:g) of pico- and nanophytoplankton, as described in section 2.4.

## 2.2. Total and size-fractionated primary productivity measurements

Pre-screened water collected from each depth of the pre-dawn casts was dispensed into Nalgene polycarbonate incubation bottles (7–8 clear bottles, plus 1 to 2 dark bottles per depth; 0.8–1.2 l each). Bottles were spiked with $^{14}$C-labeled sodium bicarbonate (PerkinElmer Health Sciences Inc.) to a final activity 0.04–0.08 μCi $ml^{-1}$. Rates of PP were calculated in units of mg C $m^{-3}$ $d^{-1}$ according to Barber et al. (1996). We included the activity of dark bottles to account for dark fixation of dissolved inorganic $^{14}$C by phytoplankton and bacteria (Banse, 1993). Bottles were incubated *in situ* at the depth of collection on a wheel-shaped polycarbonate bottle holder (one wheel per depth) (Fig. S1). Incubations were started before sunrise (usually between 05:00 and 06:00 h) and were terminated 24 h later. Filtrations for measuring total PP and size-fractionated rates of PP of the pico-, nano-, and microphytoplankton were done as described previously for the chl-*a* samples. After filtration, filters were covered with 500 μl of 0.5 N HCl and de-gassed on a shaker table for 24 h to remove unincorporated $^{14}CO_2$. Scintillation cocktail (10 ml) was added before counting in a Packard Tri-Carb 2000CA liquid scintillation analyzer.

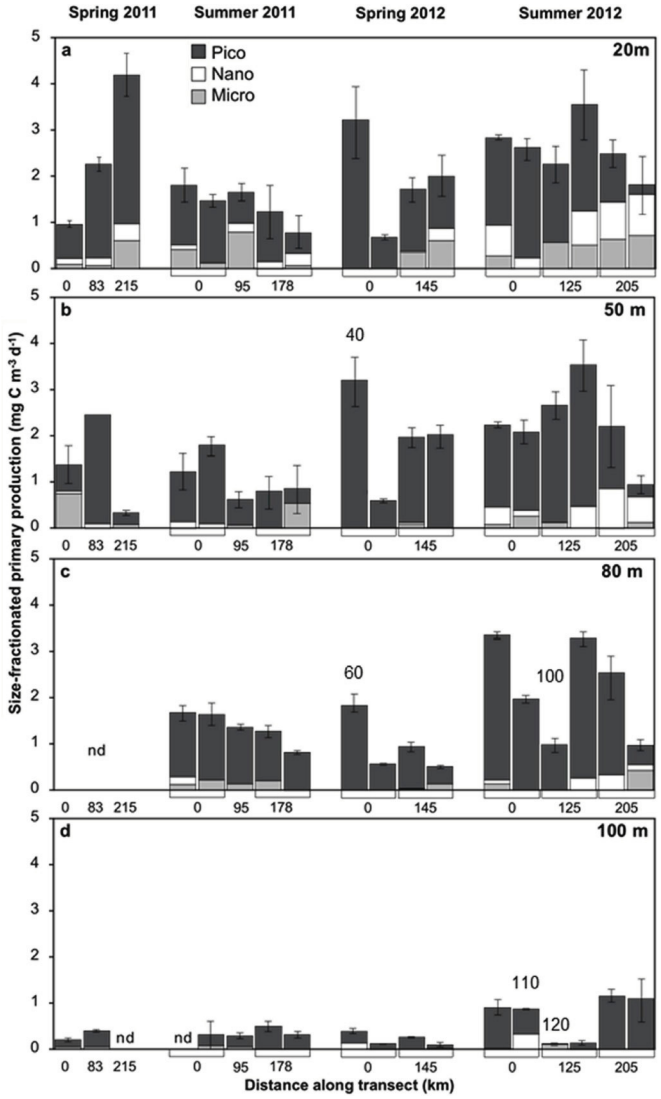


**Fig. 3.** Size-fractionated primary productivity (PP) data for the picophytoplankton (Pico), nanophytoplankton (Nano) and microphytoplankton (Micro) at: a) 20 m, b) 50 m, c) 80 m, d) 100 m (unless otherwise noted by values over individual bars). Cruise transects began at an eddy's center (0 km) and progressed to an edge station (except for Spring 2012) then to the Bermuda Atlantic Time-series Study site (farthest point along each transect). Error bars represent the standard deviation of triplicate measurements of total PP at each depth. Standard deviations for individual size fractions were ~19% of the average (range 0.1%–61%) depending on fraction, depth, and station.

**Table 3**
Average (±standard deviation, where possible) size-fractionated and total integrated (to 100 m) rates of primary productivity for all cruises and stations. All else as in Table 2.

| Cruise (Eddy) | Date | Station | Pico Productivity (mg C $m^{-2}$ $d^{-1}$) | Nano Productivity (mg C $m^{-2}$ $d^{-1}$) | Micro Productivity (mg C $m^{-2}$ $d^{-1}$) | Total Productivity (mg C $m^{-2}$ $d^{-1}$) |
|---|---|---|---|---|---|---|
| AE1102 (AC1) | Spring 2011 | Center | 52 (56%) | 6 (7%) | 35 (38%) | 93 |
| | | Edge | 174 (94%) | 9 (4%) | 5 (2%) | 188 |
| | | BATS | 123 (76%) | 13 (6%) | 25 (17%) | 161 |
| AE1118 (C1) | Summer 2011 | Center | 124 ± 17 (85%) | 8 ± 6 (5%) | 14 ± 5 (10%) | 146 ± 5 |
| | | Edge | 73 (64%) | 7 (6%) | 34 (30%) | 114 |
| | | BATS | 72 ± 32 (77%) | 7 ± 3 (8%) | 12 ± 10 (15%) | 91 ± 19 |
| AE1206 (C2) | Spring 2012 | Center | 128 ± 115 (99%) | 1 ± 2 (1%) | 0 (0%) | 129 ± 111 |
| | | BATS | 119 ± 12 (81%) | 6 ± 5 (4%) | 21 ± 7 (15%) | 146 ± 0 |
| AE1219 (AC2) | Summer 2012 | Center | 198 ± 13 (84%) | 27 ± 15 (11%) | 12 ± 6 (5%) | 236 ± 33 |
| | | Edge | 205 ± 64 (83%) | 23 ± 33 (7%) | 22 ± 5 (10%) | 250 ± 91 |
| | | BATS | 90 ± 76 (46%) | 57 ± 7 (34%) | 32 ± 12 (20%) | 178 ± 71 |

### 2.3. Analytical Methods

Samples for HPLC analysis were analyzed following the procedures described in Pinckney et al. (1996). Briefly, samples were lyophilized for 24 h at −50 °C, placed in 90% acetone (0.45–0.55 ml) and extracted at −20 °C for 24 h. Filtered extracts (350 µl) were injected into a Shimadzu HPLC. Pigment peaks were identified by comparison of retention times and absorption spectra with pure standards (DHI, Denmark). The synthetic carotenoid β-apo-8′-carotenal (Sigma) was used as an internal standard.

Flow cytometry samples were analyzed on a Becton-Dickinson Influx cytometer using 488 nm blue excitation laser with chl-*a* (692 nm) and phycoerythrin (580 nm) emission bands. Fluorescence data were collected using log amplification and recorded in relative units. Counts of cyanobacteria (*Prochlorococcus* and *Synechococcus*), pico- and nano-eukaryotes were converted to cell abundances (cells $ml^{-1}$; Sieracki et al., 1993). Relative fluorescence units (RFU $cell^{-1}$) are reported for the individual groups. We used the Casey et al. (2013) method to estimate cell carbon content ($Q_C$). That approach used cultures and natural samples collected in the Sargasso Sea to derive the following empirical relationship between 0.53 µm bead normalized forward scatter pulse height (FSC) and $Q_C$:

$$Q_C = 99.14(FSC) + 19.51 \quad (1)$$

Total particulate organic carbon (POC) biomass for specific groups (mg C $m^{-3}$) was found by multiplying cell abundances (cells $m^{-3}$) by carbon per cell (fg C $cell^{-1}$).

### 2.4. Calculations and statistical analyses

Measurements of chl-*a* biomass and PP made at discrete depths were integrated using trapezoidal integration to 100 m. We calculated assimilation numbers ($P^{Chl}$; mg C mg chl-$a^{-1}$ $d^{-1}$) for each phytoplankton size fraction by dividing PP by chl-*a* biomass. Total picophytoplankton POC (mg C $m^{-3}$) was calculated as the sum of the flow cytometry-derived POC biomass (mg C $m^{-3}$) of the specific *Prochlorococcus*, *Synechococcus,* and picoeukaryote groups described in section 2.3. Carbon:chl-*a* ratios (g $g^{-1}$) for the picophytoplankton were then calculated by dividing this sum by picophytoplankton chl-*a* biomass (mg chl-*a* $m^{-3}$). To calculate nanophytoplankton C:chl-*a* ratios, the flow cytometry-derived POC biomass of the nanoeukaryotes was divided by the nanophytoplankton chl-*a* biomass. Flow cytometry and size-fractionated chl-*a* biomass measurements were sampled on different casts (mid-day vs. pre-dawn of the same day), therefore we used the relative contributions of each size class to total chl-*a* that were measured on pre-dawn casts to derive size-fractionated chl-*a* from total chl-*a* measurements made on water from the mid-day casts. This approach makes the assumption that the contributions of the different size classes to total chl-a did not change since the pre-dawn casts.

To determine which size fraction(s) best explained the variability in total biomass and primary productivity, we performed stepwise linear regressions where total chl-*a* and total PP were the dependent variables and pico-, nano-, and microphytoplankton chl-*a* and PP rates were the independent variables.

A non-parametric Spearman Rank correlation analysis ($\alpha = 0.01$) was used to determine whether size-dependent contributions to total biomass (as chl-*a*) were proportional to size-dependent contributions to total PP. Data were pooled by size class from all cruises. Integrated measurements and those from discrete sampling depths were analyzed separately to address whether there were predictable relationships in size-dependent contributions with respect to depth.

We also calculated size-specific rates of PP by multiplying total PP by size-specific contributions to biomass - for comparison with direct measurements of PP. A paired comparisons t-test was then used to test whether there was a significant difference between measured versus calculated size-specific rates. Regression analyses allowed us to determine whether using size-fractionated biomass as an indirect way to estimate size-fractionated rates of PP for food web models is a robust approach.

All statistical analyses were performed with SPSS 24.0 software ($\alpha = 0.01$).

## 3. Results

### 3.1. Total and size-fractionated chl-a biomass

Total chl-*a* was evenly distributed through the water column in spring 2011, during a period of deep mixing (Fig. 1). On all other cruises there were detectable chl-*a* maxima between 80 and 120 m depending on the station and cruise (Fig. 1).

Picophytoplankton contributed the most to total chl-*a* biomass at all stations (Fig. 2). Over the four cruises, integrated picophytoplankton chl-*a* biomass ranged from 8 to 28 mg $m^{-2}$ which represented 53–85% of the total integrated chl-*a* depending on station and cruise (Table 2).

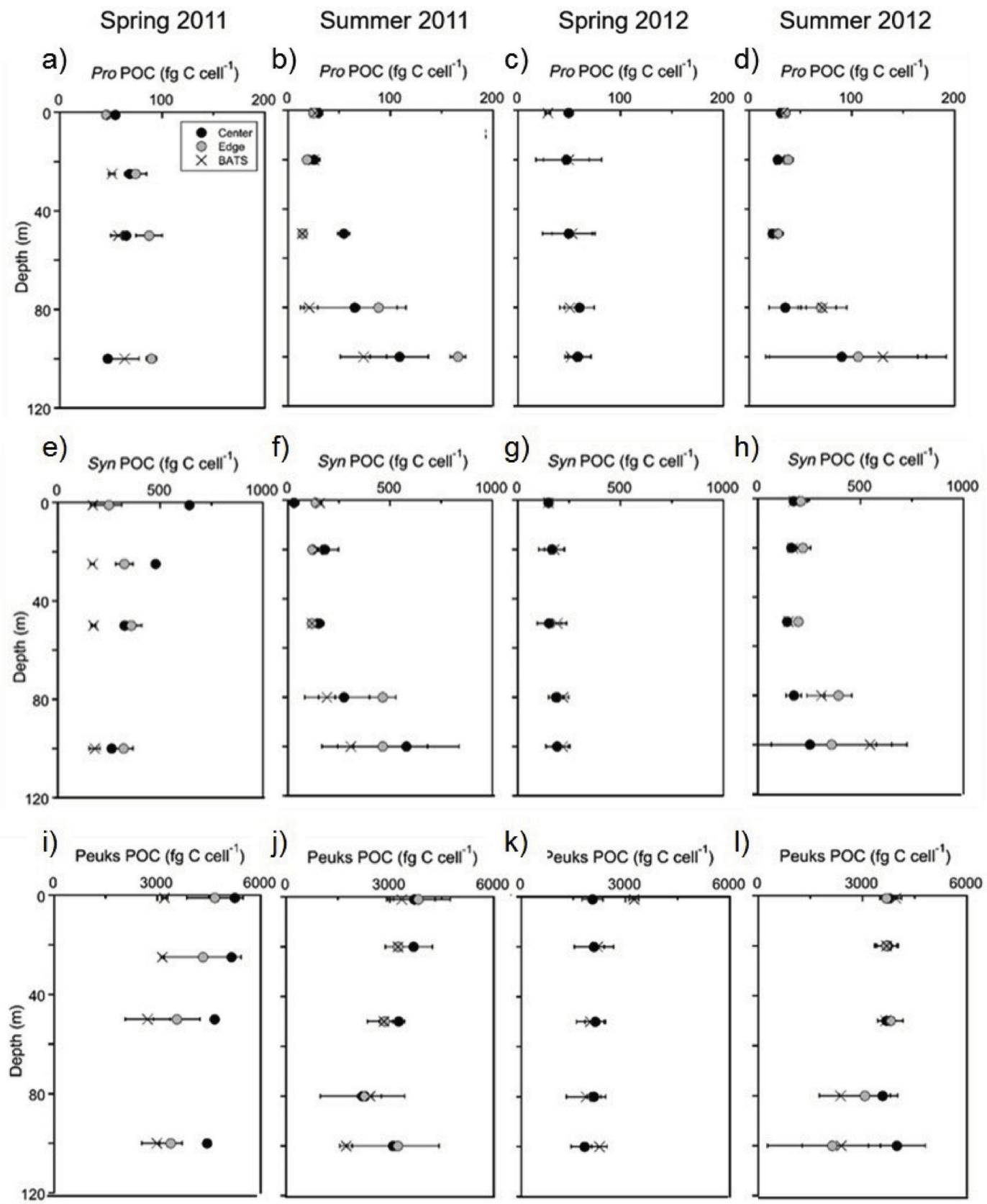


**Fig. 4.** Vertical profiles of average (±standard deviations) cell-specific POC (in fg C cell$^{-1}$) for (a–d) *Prochlorococcus* (*Pro*), (e–h) *Synechococcus* (*Syn*), and (i–l) picoeukaryotes (Peuks). Stations (eddy center, eddy edge, and the BATS station) are denoted by individual symbols; the error bars represent standard deviations between multiple casts at a given station ($n \geq 3$). Note differences in the scales of the x-axis. POC per cell was derived using flow cytometry according to Casey et al. (2013).

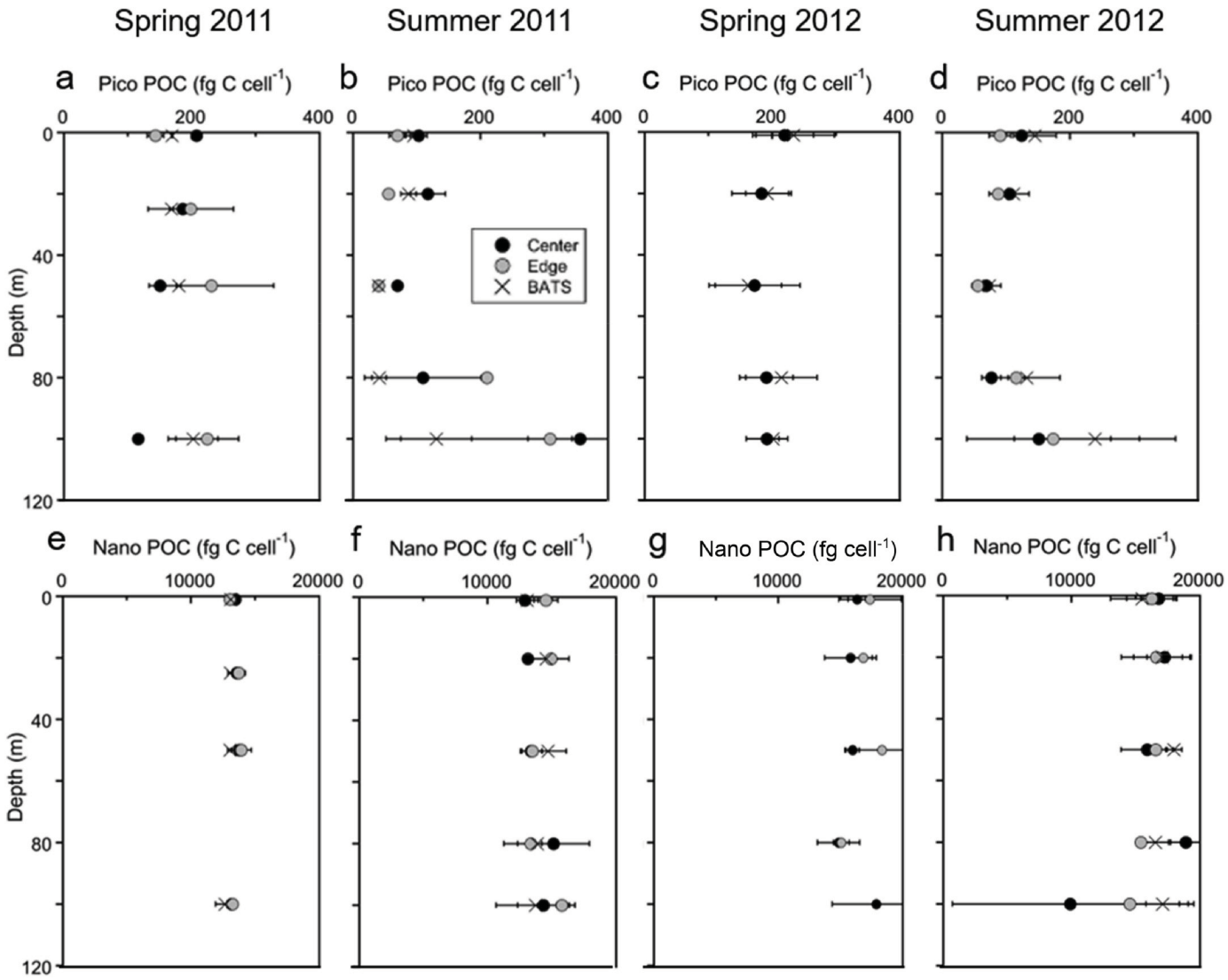


**Fig. 5.** Vertical profiles of average (±standard deviations) cell-specific POC (in fg C cell$^{-1}$) for (a–d) the combined picophytoplankton size class (*Prochlorococcus* + *Synechococcus* + picoeukaryotes = Pico POC) and the nanophytoplankton (Nano POC) (e–h). Stations (eddy center, eddy edge, and the BATS station) are denoted by individual symbols; the error bars represent standard deviations between multiple casts at a given station (n ≥ 3). Note differences in the scales of the x-axis. POC per cell was derived using flow cytometry according to Casey et al. (2013).

Multiple linear regression analysis showed that, overall, picophytoplankton biomass explained 84% of the variance in integrated total chl-*a* (Fig. S2a). Nanophytoplankton contributions varied with depth and by station for all cruises and were highest in both relative and absolute abundance in spring 2011 at the center of eddy AC1 and at the BATS station (Fig. 2, Table 2). The microphytoplankton were generally most abundant deeper in the water column, especially at the chl-*a* maximum (e.g., at 80 m in the center of eddy C1 (0 km) in summer 2011; Fig. 2c, and at the center of eddy AC2 in summer 2012; Fig. 2d).

Overall, total and size-fractionated phytoplankton biomass varied along transects from the center of each eddy to the BATS station, but there were no consistent patterns of variation within or among eddy type or season, and we often found substantial variation (>10%) in total chl-*a* even between replicate casts at the same station. This was especially true for samples collected from 80 m and 100 m in summer 2011 and spring and summer 2012 at all stations (Fig. 2c and d).

### 3.2. Total and size-fractionated primary productivity

On all cruises, depth-specific rates of PP were highest at 20 m or 50 m (to ~4 mg C m$^{-3}$ d$^{-1}$) and lowest at 100 m (<1 mg C m$^{-3}$ d$^{-1}$) (Fig. 3). Picophytoplankton made the highest absolute and relative contributions to PP (Table 3). The picophytoplankton size class was often responsible for 100% of the carbon fixed at depths at or below 80 m (Fig. 3c and d). Nanophytoplankton productivity rates were generally <0.3 mg C m$^{-3}$ d$^{-1}$ at all depths and on all cruises, except for summer 2012 when rates at 20 m were nearer to 1 mg C m$^{-3}$ d$^{-1}$ (Fig. 3a). Microphytoplankton contributions to total productivity ranged from 0 to 0.8 mg C m$^{-3}$ d$^{-1}$

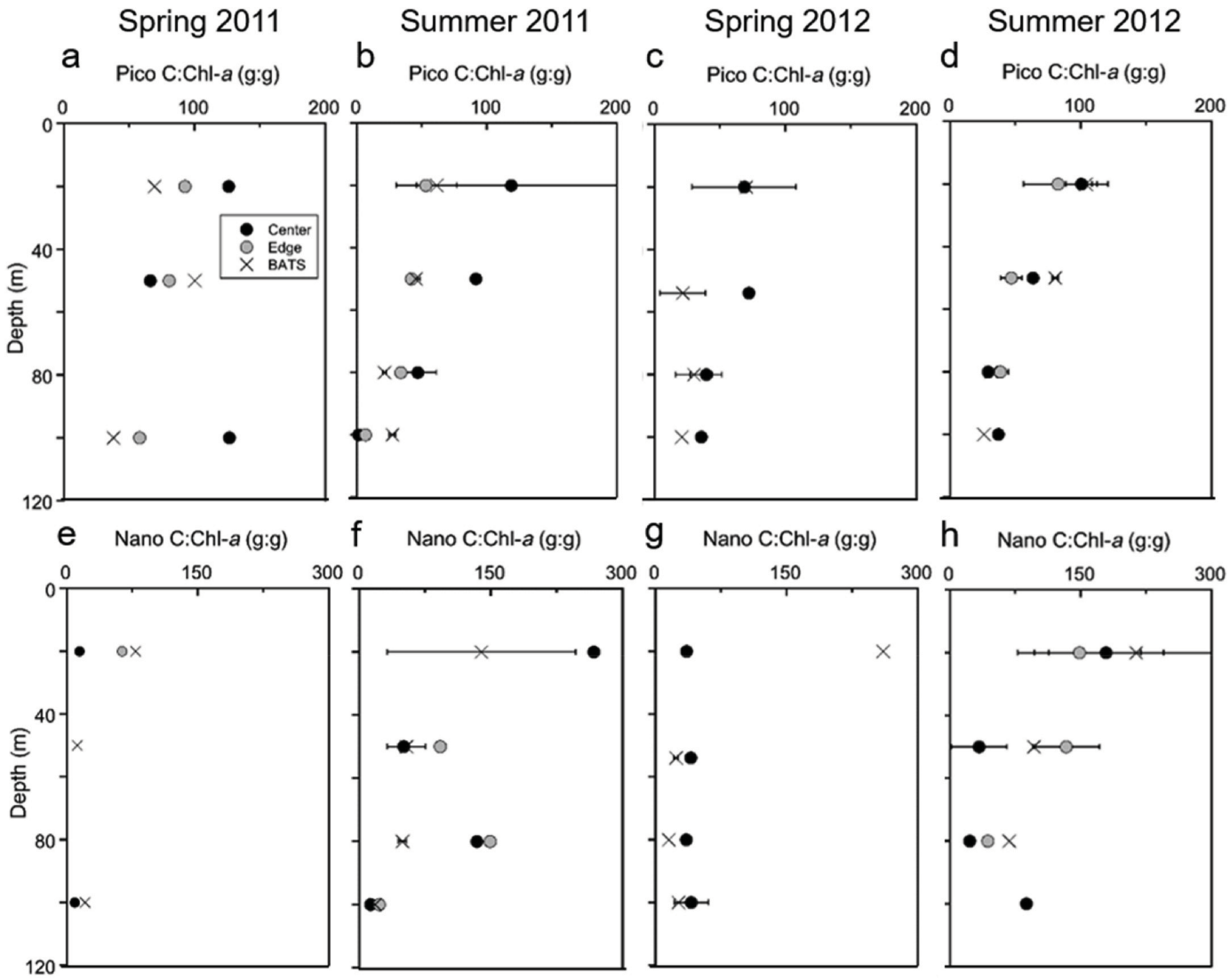


**Fig. 6.** Vertical profiles of average (±SD) cell-specific C:Chl-*a* ratios (g:g) for the (a–d) picophytoplankton (Pico) and (e–h) nanophytoplankton (Nano). These ratios were calculated from the cell-specific POC values presented in Fig. 5 (fg C cell$^{-1}$) and cell count data for each size fraction (cells m$^{-3}$; not shown). Stations (eddy center, eddy edge, and the BATS station) are denoted by individual symbols; the error bars represent standard deviations between multiple casts at a given station ($n \geq 3$). Note differences in the scales of the x-axis.

and were greatest at 20 m, in most cases (Fig. 3a).

Total integrated PP rates ranged from 91 to 350 mg C m$^{-2}$ d$^{-1}$ over all stations and cruises (Table 3). Picophytoplankton contributed 46–99% of the integrated total PP (Table 3). Contributions by the nanophytoplankton to total PP ranged from 1% to 34% and relative contributions by the microphytoplankton were 0–38%. Picophytoplankton productivity explained 87% of the variability in integrated total PP measurements (Fig. S2b).

### 3.3. Pico- and nanophytoplankton cell carbon content and C:chl-a ratios

Cellular carbon content for *Prochlorococcus*, *Synechococcus* and picoeukaryotes ranged, over all stations and depths, from 20 to 150 fg C cell$^{-1}$, 175 to 600 fg C cell$^{-1}$, and 2250 to 7500 fg C cell$^{-1}$, respectively (Fig. 4). On both spring cruises, cell carbon content was relatively uniform with depth for each of the picophytoplankton component groups (Fig. 4a, c, e, g, i, k).

Cell carbon content for the combined picophytoplankton size class (*Prochlorococcus* + *Synechococcus* + picoeukaryotes = Pico POC) was also relatively uniform with depth on the spring cruises, but increased 2 to 5-fold from 20 to 100 m in summer (Fig. 5a–d). Nanophytoplankton cell carbon content ranged from 12,000 to 18,000 fg C cell$^{-1}$ at all depths and cruises (Fig. 5e–h).

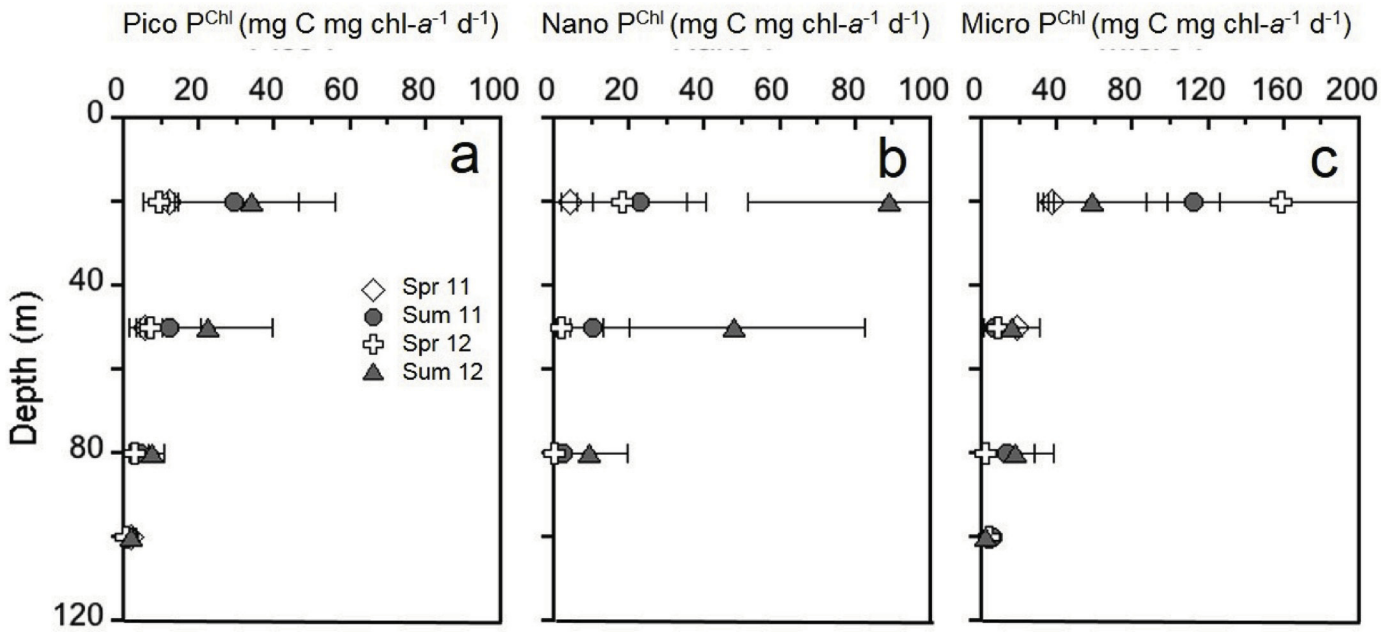


**Fig. 7.** Vertical profiles of size-fractionated assimilation numbers ($P^{Chl}$) (mg C mg chl-$a^{-1}$ $d^{-1}$) for the a) picophytoplankton (Pico), b) nanophytoplankton (Nano), and c) microphytoplankton (Micro), where error bars represent the standard deviation among casts ($n \geq 3$) on each cruise. Note differences in the x-axis scales.

### 3.4. Picophytoplankton and nanophytoplankton C:chl-a ratios

Picophytoplankton C:chl-*a* ratios decreased with depth on all cruises (Fig. 6a–d), with the possible exception of two stations in Spring 2011 (Fig. 6a). The decline with depth was most distinct in summer where C:chl-*a* ratios were >100 g:g at 20 m and decreased to ~25 g:g at 100 m (Fig. 6b, d). C:chl-*a* ratios of the nanophytoplankton size class also generally declined with depth (Fig. 6e–h), but the overall variability was higher among stations so vertical trends were not as apparent as for the picophytoplankton.

### 3.5. Assimilation numbers

Assimilation numbers ($P^{Chl}$) for all size fractions were generally greater in the surface waters and decreased with depth at all stations and on all cruises (Fig. 7). We also observed higher $P^{Chl}$ rates on summer cruises for all size fractions. Overall, the microphytoplankton had the highest assimilation numbers (from 10 to 194 mg C mg chl-$a^{-1}$ $d^{-1}$ depending on cruise). At 20 m, $P^{Chl}$ values of the microphytoplankton were significantly higher than for the picophytoplankton.

**Table 4**
Pearson's correlation coefficient (r) between the relative contributions of three size classes of phytoplankton (Pico = 0.7–2 μm; Nano = 2–20 μm; Micro = 20–200 μm) to total chlorophyll-*a* (chl-*a*) versus their relative contributions to total primary productivity (PP). Correlations were considered significant at $p < 0.05$.

| % Contribution to total chl-*a* vs. % Contribution to total PP | | | | | | | |
|---|---|---|---|---|---|---|---|
| Depth (m) | n | Pico | | Nano | | Micro | |
| | | r | *p* | r | *p* | r | *p* |
| 20 m | 18 | −0.135 | 0.593 | 0.010 | 0.967 | 0.410 | 0.093 |
| 50 m | 18 | 0.209 | 0.404 | 0.044 | 0.861 | 0.255 | 0.306 |
| 80 m | 15 | −0.169 | 0.547 | −0.350 | 0.201 | −0.060 | 0.831 |
| 100 m | 16 | 0.069 | 0.794 | −0.302 | 0.238 | 0.091 | 0.729 |
| Integrated | 18 | 0.080 | 0.771 | −0.221 | 0.380 | 0.040 | 0.894 |

## 4. Discussion

Our results, and those of the few studies that have examined size-specific contributions in the Sargasso Sea (Prézelin and Glover, 1991; Malone et al., 1993; Goericke, 1998), convincingly show that picophytoplankton dominate both biomass and total PP in this region. While this dominance was not surprising, the finding that changes in the picophytoplankton size-class explained 84% of the variance in total integrated chl-*a* and 87% of the variance in total PP was somewhat unexpected. Historically, picophytoplankton have been thought to exist as an "unchanging background", with variability in biomass and carbon fixation being driven by the larger phytoplankton groups (Raimbault et al., 1988). Our results are therefore more similar to those of Marañón et al. (2001), who found that picophytoplankton explained 61% or more of the total variance in primary production in oligotrophic regions (defined by them as regions with integrated chl-$a < 40$ mg $m^{-2}$). The Marañón et al. (2001) study appears to be the first to recognize that temporal and spatial variability in total biomass and total PP may not always be driven by changes in the larger size fractions. Our data support those of Marañón et al. and subsequent studies (Fernández et al., 2003; Marañón et al., 2003; Moreno-Ostos et al., 2011) that credit the picophytoplankton with driving the underlying dynamics of oligotrophic communities.

Our data also clearly demonstrate the well-documented seasonal hydrography of the Sargasso Sea (Steinberg et al., 2001; Lomas et al., 2013): deep winter/spring mixing driven by convection and thermal stratification in summer. Deep chlorophyll maxima were observed near the base of the euphotic zone so that total chl-*a* increased with depth in response to lower light availability and the lack of vertical mixing through the entire euphotic zone (see Cullen, 1982, 2015). Although in summer the majority of chl-*a* biomass was at or below 80 m, 84% of the carbon fixation occurred above these depths, at all times. On our summer cruises, low PP (<1 mg C $m^{-3}$ $d^{-1}$) suggested that DCM communities were not highly active, providing a clear example of low light photoacclimation resulting in a disproportional relationship between chl-*a* biomass and PP. These vertical differences resulted in higher assimilation numbers calculated for surface waters for all size classes

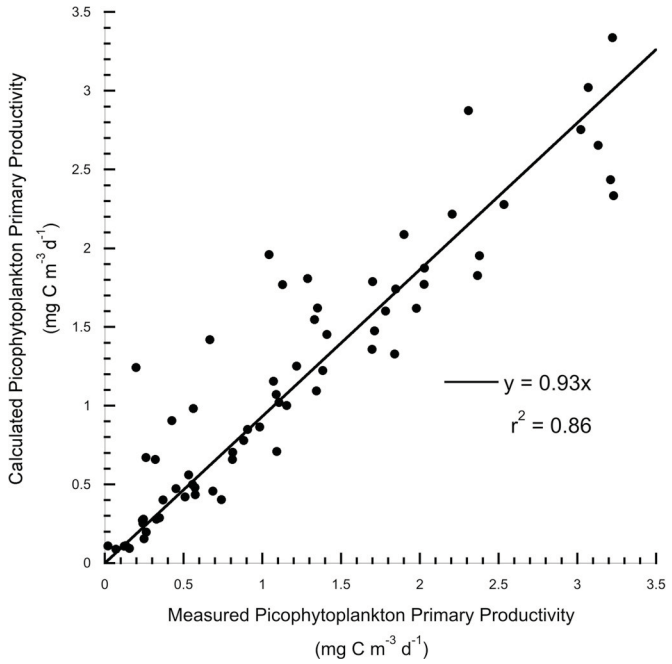


**Fig. 8.** Rates of primary productivity (PP) for picophytoplankton from the Sargasso Sea estimated by calculating total rates of PP by size-fractionated chl-*a* biomass concentrations, versus rates measured directly by size-fractionated $^{14}C$ incubation experiments. Using biomass to apportion size-specific rates of PP results in a 7% average underestimate of picophytoplankton contributions to total PP.

(between 10 and 125 mg C mg chl-$a^{-1}$ $d^{-1}$). Nano- and microphytoplankton contributed their largest fraction of PP in the upper 50 m, though the majority of their biomass was found at depths of 80 and 100 m. Therefore, the assimilation numbers of these size classes often exceeded picophytoplankton in surface waters.

Previous studies in oligotrophic waters have shown that large eukaryotes have higher $P^{Chl}$ than picophytoplankton in surface waters (Fernández et al., 2003; Marañón, 2005; Poulton et al., 2006). Here, microphytoplankton $P^{Chl}$ at 20 m was usually greater than that of the pico- and nanophytoplankton. Differences in the C:chl-*a* ratios of individual size fractions may drive differences in the $P^{Chl}$ rates we measured. Though we could not calculate microphytoplankton C:chl-*a* directly, we did observe differences between the pico- and nanophytoplankton C:chl-*a* ratios. In summer, for example, nanophytoplankton C:chl-*a* ratios often exceeded 200 (g:g) in surface waters while picophytoplankton C:chl-*a* ratios were between 50 and 150 (g:g). The correspondingly lower picophytoplankton $P^{Chl}$ was likely the result of lower pigment packaging in the picophytoplankton. The packing of individual pigment molecules within a cell decreases the specific absorption efficiency relative to pigments in solution (Duysens, 1956; Morel and Bricaud, 1981) and is positively related to cell size (Ciotti et al., 2002). In bright surface waters, self-shading is beneficial as it helps prevent photoinhibition (Berner et al., 1989). There were no significant differences in size-dependent $P^{Chl}$ at the DCM, where $P^{Chl}$ for all size fractions was <10 mg C mg chl-$a^{-1}$ $d^{-1}$. As mentioned earlier, this is likely because phytoplankton tend to increase intracellular chl-*a* concentrations in response to low light (see also Raven, 1998; Letelier et al., 2004). We should acknowledge that errors introduced by combining flow cytometry and filter-based approaches may contribute to uncertainty in C:chl-*a* ratios (and hence $P^{Chl}$), as would errors associated with filtration-based size fractionation including cell breakage and inefficient capture of the targeted size range of phytoplankton (see Azam, 1998; Azam et al., 1983, 1993; Banse, 1993; Barber et al., 1996; Boyd and Newton, 1995; Ducklow et al., 1986; Koestner et al., 2019; Legendre and Le Fèvre, 1989, 1991; Malone, 1980; Marañón et al., 2001; McManus, 1991; Michaels and Silver, 1988; Nayar and Chou, 2003; Pinckney et al., 1996; Pomeroy, 1974; Rivkin et al., 1996; Robinson and Williams, 2005; Ryther, 1969; Sieracki et al., 1993; Tremblay and Legendre, 1994).

The grouping of phytoplankton into "pico", "nano", and "micro" size classes does not account for variability associated with different strains, species, or even ecotypes of the same species. For example, in summer we found the cell carbon content of *Prochlorococcus* was 4x greater at 100 m compared to concentrations in surface waters. The observed increase in *Prochlorococcus* cell carbon is likely due to the strong vertical partitioning that occurs under stratified conditions, whereby predominantly low-light adapted ecotypes dominate deeper in the water column (Coleman and Chisholm, 2007). Low light *Prochlorococcus* ecotypes have larger genomes and larger cell sizes and carbon content, as compared to high light adapted ecotypes that dominate surface waters (Biller et al., 2015).

Seasonal shifts in hydrography as described above act gradually, while mesoscale eddies, occurring over spatial scales <100 km, vertically displace the water column structure on timescales of days to weeks (McGillicuddy and Robinson, 1997). The interaction of wind on surface waters along eddy perimeters leads to upwelling events that last less than a week (Klein and Lapeyre, 2009), while internal waves may occur on diel timescales (Owen, 1981); both processes displace phytoplankton communities along isopycnal gradients (Liccardo et al., 2013). We believe that the interaction between two eddies in summer 2012 promoted sub-mesoscale turbulence that temporarily injected nutrients into

the euphotic zone (e.g., Klein et al., 2008) and generated a response in the larger phytoplankton size classes. Under these conditions, the phytoplankton >2 μm in size had the highest assimilation numbers we measured, and were responsible for up to 54% of total PP though they represented <25% of the total chl-*a*. However, while the response of larger phytoplankton to changing environmental conditions can modify community size structure on the short term (Poulton et al., 2006), we still found that the picophytoplankton dominated phytoplankton standing stocks at all times.

When presenting our data, we plotted profiles for each station (and casts at the same station) separately because of the eddy-related variability in physical conditions at each sampling point. Substantial natural variability was evident even between measurements taken from sequential casts at a single station. Our profiles of chl-*a* illustrate this point clearly. For example, in spring 2012, the chlorophyll maximum at ~80 m at the BATS station was a chlorophyll minimum at that depth by the next sampling event, 48 h later (Fig. 1). Though this created challenges for interpreting these data, our cruise plans were designed to sample across diverse environmental conditions over a relatively short time frame (~2 weeks), using eddies as natural laboratories – and we were successful in capturing this variability.

The importance of physical forcing described above cannot be overstated as it dictates conditions experienced by the resident phytoplankton communities. As water column structure can change over short timescales, this could be problematic when combining flow cytometry-derived carbon biomass data and total chl-*a* from one cast (mid-day) with size-fractions of chl-*a* estimated from pre-dawn productivity casts. To minimize potential errors associated with this, we did core casts in the same water mass as soon as possible after productivity casts. We evaluated size-fractionated chl-*a* measurements taken from successive productivity casts and found the relative contributions of each size class to total chl-*a* changed by less than 20%.

Accurate representations of phytoplankton community structure and function are critical for constructing realistic plankton food web models (e.g., Vézina and Platt, 1988; Marquis et al., 2011). When size-fractionated productivity rates are unavailable, the productivity of individual size fractions must often be estimated from size-specific contributions to total chl-*a* biomass (e.g., Daniels et al., 2006; Richardson et al., 2006; Vernet et al., 2017). Our results for the Sargasso Sea illustrate a potential problem with this approach: we found no significant correlations for any size class between the relative contributions to total chl-*a* and to total PP for discrete depth measurements or for integrated values (Table 4). This indicates that size-fractionated chl-*a* measurements alone are not sufficient to investigate variability in the relative contributions of various size classes to PP in the Sargasso Sea, and that size-dependent assimilation numbers are instead the most important driver. However, if we wish to estimate the absolute contribution of a size class to total PP, the relative contributions of a size class to total chl-*a* are useful. When we compared size fractionated rates of PP measured directly to those calculated by multiplying the total PP by the relative contributions of each size class to chl-*a*, we found no significant difference between measured and calculated rates when all size fractions were considered together (paired t-test; $p = 0.999$, $df = 200$), or separately (picophytoplankton $p = 0.664$, $df = 66$; nanophytoplankton $p = 0.072$, $df = 66$; microphytoplankton $p = 0.161$, $df = 66$). For the picophytoplankton, the regression of calculated vs. measured primary productivity had a slope of 0.93 ($r^2 = 0.86$; residual standard deviation = 0.31) indicating a tendency to underestimate picophytoplankton PP (by 7%) if estimated using biomass instead of direct PP measurements (Fig. 8). Note that this is an average underestimate that is influenced by the greater scatter at higher rates of primary productivity. In contrast, the nanophytoplankton regression slope was 0.31 ($r^2$=0.09, residual standard deviation = 0.20) and the microphytoplankton regression slope was 0.22 (r2=0.05, residual mean standard deviation of 0.14) indicating little support for this approach for these two size classes. Using relative contributions to chl-*a* as a way to apportion total PP could be done with reasonable confidence for the picophytoplankton, because this size class was responsible for such a large percentage of the variance in both biomass and PP. We propose, therefore, that the use of size-fractionated chl-*a* as an estimator of size-fractionated rates of primary productivity could be done with confidence in any ecosystem where picophytoplankton dominate both biomass and primary productivity.

## 5. Summary

Our study of size-fractionated biomass and PP in the Sargasso Sea had both expected and unanticipated results. As expected, the picophytoplankton (*Synechococcus*, *Prochlorococcus*, and picoeukaryotes) together accounted for greater than 53% of the total integrated chl-*a* and 46% or more of the total integrated PP. Unexpectedly, variations in the picophytoplankton size-class explained 84% of the variance in total integrated chl-*a* and 87% of the variance in total PP, indicating that variability in the Sargasso Sea is not always driven by changes in the larger phytoplankton size category. Size-dependent relative contributions to biomass versus PP varied with depth, with differences generally driven by vertical (and therefore photoacclimation or taxonomic) variations in C:chl-*a* ratios and chlorophyll-specific rates of PP. We found no significant correlations between size-dependent contributions to chl-*a* biomass versus PP overall. For the picophytoplankton, using relative contributions to biomass resulted in an underprediction of their contributions to total primary productivity by 7%, and would therefore be a good proxy for size-dependent contributions to PP for cases where size-fractionated rates of PP were not available.

## Declaration of competing interest

None.

## Acknowledgements

Funding for this project came from the National Science Foundation (OCE-1030345 to TLR) and the Slocum Lunz Foundation (to BCR). We thank Debra Lomas and Douglas Bell for valuable technical support, and the Captain, marine technicians, and crew of the R/V *Atlantic Explorer* for expert assistance at sea.

## Appendix A. Supplementary data

Supplementary data to this article can be found online at https://doi.org/10.1016/j.dsr.2019.103141.

## References

Azam, F., Fenchel, T., Field, J.G., Gray, J.S., Meyer-Reil, L.A., Thingstad, F., 1983. The ecological role of water-column microbes in the sea. Mar. Ecol. Prog. Ser. 10, 257–263.

Azam, F., Smith, D.C., Steward, G.F., Hagstrom, A., 1993. Bacteria-organic matter coupling and its significance for oceanic carbon cycling. Microb. Ecol. 28, 167–197.
Azam, F., 1998. Microbial control of oceanic carbon flux: the plot thickens. Science 280, 694–696.
Banse, K., 1993. On the dark bottle in the $^{14}$C method for measuring marine phytoplankton production. ICES Mar. Sci. Symp. 197, 132–140.
Barber, R.T., Sanderson, M.P., Lindley, S.T., Chai, F., Newton, J., Trees, C.C., Foley, D.G., Chavez, F.P., 1996. Primary productivity and its regulation in the equatorial Pacific during and following the 1991-1992 El-Niño. Deep Sea Res. II 43, 933–969.
Berner, T., Dubinsky, Z., Wyman, K., Falkowski, P.G., 1989. Photoadaptation and the "package" effect in *Dunaliella tertiolecta* (Chlorophyceae). J. Phycol. 25, 70–78.
Biller, S.J., Berube, P.M., Lindell, D., Chisholm, S.W., 2015. *Prochlorococcus*: the structure and function of collective diversity. Nat. Rev. 13, 13–27.
Boyd, P.W., Newton, P.P., 1995. Evidence of the potential influence of planktonic community structure on the inter-annual variability of particulate organic carbon flux. Deep Sea Res. I 42, 619–639.
Bruno, S.F., Staker, R.D., Sharma, G.M., Turner, J.T., 1983. Primary productivity and phytoplankton size fraction dominance in a temperate North Atlantic estuary. Estuaries 6, 200–211.
Casey, J.R., Aucan, J.P., Goldberg, S.R., Lomas, M.W., 2013. Changes in partitioning of carbon amongst photosynthetic pico- and nano-plankton groups in the Sargasso Sea in response to changes in the North Atlantic Oscillation. Deep Sea Res. II 93, 58–70.
Ciotti, A.M., Lewis, M.R., Cullen, J.J., 2002. Assessment of the relationships between dominant cell size in natural phytoplankton communities and the spectral shape of the absorption coefficient. Limnol. Oceanogr. 47, 404–417.
Coleman, M.L., Chisholm, S.W., 2007. Code and context: *Prochlorococcus* as a model for cross-scale biology. Trends Microbiol. 15, 398–407.
Cotti-Rausch, B.E., Lomas, M.W., Lachenmyer, E.M., Bell, D.W., Goldberg, S.R., Richardson, T.L., 2016. Mesoscale and sub-mesoscale variability in phytoplankton community composition in the Sargasso sea. Deep Sea Res. I 110, 106–122.
Cullen, J.J., 1982. The deep chlorophyll maximum: comparing vertical profiles of chlorophyll *a*. Can. J. Fish. Aquat. Sci. 39, 791–803.
Cullen, J.J., 2015. Sub-surface chlorophyll maximum layers: enduring enigma or mystery solved? Ann. Rev. Mar. Sci. 7, 207–239.
Daniels, R.M., Richardson, T.L., Ducklow, H.W., 2006. Food web structure and biogeochemical processes during oceanic phytoplankton blooms: an inverse model analysis. Deep Sea Res. II 53, 532–554.
De Martini, F., 2016. Growth and Grazing Mortality of Pico-And Nano-Phytoplankton and Their Role in the Carbon Export in the Sargasso Sea. Doctoral Dissertation. Arizona State University, Tempe, p. 187.
Ducklow, H.W., Purdie, D.A., Williams, P.J. LeB., Davies, J.M., 1986. Bacterioplankton: a sink for carbon in a coastal marine plankton community. Science 232, 865–867.
Duysens, L.N.M., 1956. The flattening of the absorption spectrum of suspensions, as compared to that of solutions. Biochim. Biophys. Acta 19, 1–12.
Ebersbach, F., Trull, T.W., 2008. Sinking particle properties from polyacrylamide gels during the KErguelen Ocean and Plateau compared Study (KEOPS): zooplankton control of carbon export in an area of persistent natural iron inputs in the Southern ocean. Limnol. Oceanogr. 53, 212–224.
Ebersbach, F., Assmy, P., Martin, P., Schulz, I., Wolzenburg, S., Nöthig, E.-M., 2014. Particle flux characterisation and sedimentation patterns of protistan plankton during the iron fertilisation experiment LOHAFEX in the Southern Ocean. Deep Sea Res. I 89, 94–103.
Fernández, E., Marañón, E., Morán, X.A.G., Serret, P., 2003. Potential causes for the unequal contribution of picophytoplankton to total biomass and productivity in oligotrophic waters. Mar. Ecol. Prog. Ser. 254, 101–109.
Furnas, M.J., 1983. Community structure, biomass and productivity of size-fractionated summer phytoplankton populations in lower Narragansett Bay, Rhode Island. J. Plankton Res. 5, 637–655.
Goericke, R., 1998. Response of phytoplankton community structure and taxon-specific growth rates to seasonally varying physical forcing in the Sargasso Sea off Bermuda. Limnol. Oceanogr. 43, 921–935.
Glover, H.E., Smith, A.E., Shapiro, L., 1985. Diurnal variations in photosynthetic rates: comparisons of ultraphytoplankton with a larger phytoplankton size fraction. J. Plankton Res. 7, 519–535.
Jochem, F.J., Zeitzschel, B., 1993. Productivity regime and phytoplankton size structure in the tropical and subtropical North Atlantic. Deep Sea Res. 40, 495–519.
Klein, P., Hua, B., Lapeyre, G., Capet, X., Le Gentil, S., Sasaki, H., 2008. Upper ocean turbulence from high 3D resolution simulations. J. Phys. Oceanogr. 38, 1748–1763.
Klein, P., Lapeyre, G., 2009. The oceanic vertical pump induced by mesoscale and submesoscale turbulence. Ann. Rev. Mar. Sci. 1, 351–375.
Legendre, L., Le Fèvre, J., 1989. New production and export of organic matter in the deep ocean: consequences of some recent recoveries. Limnol. Oceanogr. 34, 1374–1380.
Legendre, L., Le Fèvre, J., 1991. From individual plankton to pelagic marine ecosystems and to global biogeochemical cycles. In: Demers, S. (Ed.), Particle Analysis in Oceanography. Springer-Verlag, Berlin, pp. 261–299.
Koestner, D., Stramski, D., Reynolds, R.A., 2019. Assessing the effects of particle size and composition on light scattering through measurements of size-fractionated seawater samples. Limnol. Oceanogr. https://doi.org/10.1002/lno.11259.
Legendre, L., Gosselin, M., Hirche, H.-J., Kattner, G., Rosenberg, G., 1993. Environmental control and potential fate of size-fractionated phytoplankton production in the Greenland Sea (75° N). Mar. Ecol. Prog. Ser. 98, 297–313.
Letelier, R.M., Karl, D.M., Abbott, M.R., Bidigare, R.B., 2004. Light driven seasonal patterns of chlorophyll and nitrate in the lower euphotic zone of the North Pacific Subtropical Gyre. Limnol. Oceanogr. 49, 508–519.
Liccardo, A., Fierro, A., Iudicone, D., Bouruet-Aubertot, P., Dubroca, L., 2013. Response of the deep chlorophyll maximum to fluctuations in vertical mixing intensity. Prog. Oceanogr. 109, 33–46.
Lomas, M.W., Bates, N.R., Johnson, R.J., Knap, A.H., Steinberg, D.K., Carlson, C.A., 2013. Two decades and counting: 24-years of sustained open ocean biogeochemical measurements in the Sargasso sea. Deep Sea Res. II 93, 16–32.
Malone, T.C., 1971. The relative importance of nannoplankton and netplankton as primary producers in tropical oceanic and neritic phytoplankton communities. Limnol. Oceanogr. 16, 633–639.
Malone, T.C., 1980. Algal size. In: Morris, L. (Ed.), The Physiological Ecology of Phytoplankton. University of California Press, Berkeley, pp. 433–463.
Malone, T.C., Pike, S.E., Conley, D.J., 1993. Transient variations in phytoplankton productivity at the JGOFS Bermuda time series station. Deep Sea Res. I 40, 903–924.
Marañón, E., 2005. Phytoplankton growth rates in the Atlantic subtropical gyres. Limnol. Oceanogr. 50, 299–310.
Marañón, E., Holligan, P.M., Barciela, R., González, N., Mouriño, B., Pazó, M.J., Varela, M., 2001. Patterns of phytoplankton size structure and productivity in contrasting open-ocean environments. Mar. Ecol. Prog. Ser. 216, 43–56.
Marañón, E., Behrenfeld, M.J., González, N., Mouriño, B., Zubkov, M.V., 2003. High variability of primary production in oligotrophic waters of the Atlantic Ocean: uncoupling from phytoplankton biomass and size structure. Mar. Ecol. Prog. Ser. 257, 1–11.
Marquis, E., Niquil, N., Vézina, A.F., Petitgas, P., Dupuy, C., 2011. Influence of planktonic food web structure on a system's capacity to support pelagic production: an inverse analysis approach. J. Mar. Sci. 68, 803–812.
McGillicuddy, D.J., Robinson, A.R., 1997. Eddy induced nutrient supply and new production in the Sargasso sea. Deep Sea Res. I 44, 1427–1449.
McManus, G.B., 1991. Flow analysis of a planktonic microbial food web model. Mar. Microb. Food Webs 5, 145–160.
Michaels, A.F., Silver, M.W., 1988. Primary production, sinking fluxes and the microbial food web. Deep Sea Res. I 35, 473–490.
Morel, A., Bricaud, A., 1981. Theoretical results concerning light absorption in a discrete medium, and application to specific absorption of phytoplankton. Deep Sea Res. 28, 1375–1393.
Moreno-Ostos, E., Fernández, A., Huete-Ortega, M., Mouriño-Carballido, B., Calvo-Díaz, A., Morán, X.A.G., Marañón, E., 2011. Size-fractionated phytoplankton biomass and production in the tropical Atlantic. Sci. Mar. 75, 379–389.
Motwani, N.H., Gorokhova, E., 2013. Mesozooplankton grazing on picocyanobacteria in the Baltic Sea as inferred from molecular diet analysis. PLoS One 8. https://doi.org/10.1371/journal.pone.0079230 e.79230.
Nayar, S., Chou, L.M., 2003. Relative efficiencies of different filters in retaining phytoplankton for pigment and productivity studies. Estuar Coast Shelf S. 58, 241–258.
Olson, D.B., 1991. Rings in the ocean. Annu. Rev. Earth Planet Sci. 19, 283–311.
Owen, R.W., 1981. Fronts and eddies in the sea: mechanisms, interactions and biological effects. In: Longhurst, A.R. (Ed.), Analysis of Marine Ecosystems. Academic Press, New York, pp. 197–233.
Pinckney, J.L., Millie, D.F., Howe, K.E., Paerl, H.W., Hurley, J.P., 1996. Flow scintillation counting of $^{14}$C-labeled microalgal photosynthetic pigments. J. Plankton Res. 18, 1867–1880.
Pomeroy, L.R., 1974. The ocean's food web, a changing paradigm. Bioscience 24, 499–504.
Pomeroy, L.R., Williams, P.J. leB., Azam, F., Hobbie, J.E., 2007. The microbial loop. Oceanography 20, 28–33.
Poulton, A.J., Holligan, P.M., Hickman, A., Kim, Y.-N., Adey, T.R., Stinchcombe, M.C., Holeton, C., Root, S., Woodward, E.M.S., 2006. Phytoplankton carbon fixation, chlorophyll-biomass and diagnostic pigments in the Atlantic ocean. Deep Sea Res. II 53, 1593–1610.
Prézelin, B.B., Glover, H.E., 1991. Variability in time/space estimates of phytoplankton, biomass and productivity in the Sargasso sea. J. Plankton Res. 13S, 45–67.
Raimbault, P., Rodier, M., Taupier-Letage, I., 1988. Size fraction of phytoplankton in the Ligurian Sea and the Algerian Basin (Mediterranean Sea): size distribution versus total concentration. Mar. Microb. Food Webs 3, 1–7.
Raven, J.A., 1998. The 12$^{th}$ Tansley lecture. Small is beautiful: the picophytoplankton. Funct. Ecol. 12, 503–513.
Richardson, T.L., Jackson, G.A., Ducklow, H.W., Roman, M.R., 2006. Spatial and seasonal patterns of carbon cycling through planktonic food webs of the Arabian Sea determined by inverse analysis. Deep Sea Res. II 53, 555–575.
Richardson, T.L., 2019. Mechanisms and pathways of small-phytoplankton export from the surface ocean. Annu. Rev. Mar. Sci. 11, 57–74.
Rivkin, R.B., Legendre, L., Deibel, D., Tremblay, J.-E., 1996. Vertical flux of biogenic carbon in the ocean: is there food web control? Science 272, 1163–1166.

Robinson, C., Williams, P.J. leB., 2005. Respiration and its measurement in surface marine waters. In: del Giorgio, P.A., Williams, P.J. leB. (Eds.), Respiration in Aquatic Ecosystems. Oxford University Press, Oxford, pp. 147–180.
Ryther, J., 1969. Photosynthesis and fish production in the sea. Science 166, 72–76.
Sieracki, M.E., Verity, P.G., Stoecker, D.K., 1993. Plankton community response to sequential silicate and nitrate depletion during the 1989 North-Atlantic spring bloom. Deep Sea Res. II 40, 213–225.
Steinberg, D.K., Carlson, C.A., Bates, N.R., Johnson, R.J., Michaels, A.F., Knap, A.H., 2001. Overview of the US JGOFS Bermuda Atlantic Time-series Study (BATS): a decade-scale look at ocean biology and biogeochemistry. Deep Sea Res. I 48, 1405–1447.
Sutherland, K.R., Madin, L.P., Stocker, R., 2010. Filtration of submicrometer particles by pelagic tunicates. Proc. Natl. Acad. Sci. 107, 15129–15134.
Tremblay, J.-E., Legendre, L., 1994. A model for the size-fractionated biomass and production of marine phytoplankton. Limnol. Oceanogr. 39, 2004–2014.
Vernet, M., Richardson, T.L., Metfies, K., Nöthig, E.-M., Peeken, I., 2017. Models of plankton community changes during a warm water anomaly in Arctic waters show altered pathways with minimal changes in carbon export. Front. Mar. Sci. 4, 160. https://doi.org/10.3389/fmars.2017.00160.
Vézina, A.F., Platt, T., 1988. Food web dynamics in the ocean. I. Best-estimates of flow networks using inverse methods. Mar. Ecol. Prog. Ser. 42, 269–287.
Wilson, S.E., Steinberg, D.K., 2010. Autotrophic picoplankton in mesozooplankton guts: evidence of aggregate feeding in the mesopelagic zone and export of small phytoplankton. Mar. Ecol. Prog. Ser. 412, 11–27.